Cross-Coupling Effects Mitigation in Triple Active Bridge Converter using RBFNN-Based Sliding Mode Control

Mohammed B. Debbat, Khaled Laadjal, Andres Camilo Henao-Muñoz,
Antonio Pepiciello and José L. Domínguez- García
Catalonia Institute for Energy Research (IREC), Barcelona, Spain
(mbdebbat, klaadjal, achenao, aPepiciello, jldominguez)@irec.cat

***Abstract*—This paper addresses the design of a radial basis function neural network (RBFNN)-based sliding mode control (SMC) approach to mitigate cross-coupling effects in a triple active bridge (TAB) converter. Based on a reduced-order model (ROM), a conventional SMC is first designed; subsequently, an RBFNN is employed to estimate the lumped disturbance term – representing cross-coupling effects and system uncertainties – in real time. Simulation results obtained using MATLAB/Simulink show that the proposed hybrid approach achieves effective decoupled power flow control with a fast transient response across four operating mode scenarios. A comparative analysis reveals that the proposed RBFNN-SMC substantially reduces cross-coupling effects relative to conventional SMC and PI control, offering a faster transient response and superior disturbance rejection. Furthermore, the hybrid architecture maintains a robust stability margin under parametric uncertainties, outperforming conventional PI control in decoupling bandwidth and overall transient response.**

***Index Terms*—Multiport converter, cross-coupling effects, Sliding mode control, Radial basis function neural networks.**

I. Introduction

As distributed power systems grow rapidly–integrating renewable energy sources, DC microgrids, and EV charging stations–the multi-port converter (MPC) is positioned as a promising solution, providing a single, compact power electronic interface to manage multiple sources and loads simultaneously [2]. Among other MPC topologies, the triple active bridge (TAB) has gained prominence due to its galvanic isolation, high power density, bidirectional power flow capability, and ease of soft-switching implementation [3], [4]. The TAB extends the dual active bridge (DAB) converter by using a three-winding high-frequency transformer (HFT) to integrate a third port. The presence of an HFT results in strongly coupled power flow among ports. Therefore, developing effective control strategies to suppress these cross-coupling effects presents both a necessity and a significant challenge.

To mitigate cross-coupling effects and achieve decoupled power flow in TAB converters, existing solutions generally fall into two categories: hardware-based and software-based [5], [6]. Among the software-based approaches, conventional techniques typically rely on two strategies. The first simply adds model-based feedforward terms—based on current estimations—to linear PI controllers [7]. The second uses decoupling matrices from linearized reduced-order models to cancel out cross-coupling [8], [9]. These linear control approaches are inherently constrained by their reliance on a fixed operating point, limited bandwidth, and parameter sensitivity. To overcome these issues, advanced control strategies offer a more effective solution. In [10], the authors used hardware-based sliding mode control (SMC) to enhance decoupled power flow, and in [11], cross-coupling effects are treated as a disturbance, for which an extended state observer (ESO) is designed to estimate and cancel it in real time. A hybrid approach combining diagonal matrix decoupling with differential flatness control is employed in [12] to decouple power flow and improve the dynamic performance of a TAB converter. Techniques based on artificial intelligence [13], [14] show promise in decoupling power flows, providing a solution to overcome the issues of model dependency and computational complexity.

Despite the merits of these advanced techniques, many still face challenges such as reliance on accurate system models, high computational burden, or limited ability to handle real-time disturbances. To overcome these limitations, this paper presents the design of a radial basis function neural network (RBF-NN)-based sliding mode control (SMC) approach to mitigate cross-coupling effects in a TAB converter. This hybrid technique leverages the RBFNN's ability to accurately estimate cross-coupling dynamics in real time while retaining the robustness, fast response, and ease of implementation inherent to SMC. The rest of the paper is organized as follows. In Section II, the mathematical model of TAB converter is presented. The hybrid controller combining RBFNN and SMC is derived in Section III. Simulation results of the controller, under normal and abnormal conditions are illustrated in Section IV. Finally, conclusions are given in Section VI.

II. Mathematical Modeling of TAB Converter

Fig. 1-a depicts the topology of the isolated TAB converter. It consists of three full bridges (FBs) linked through a three-winding high-frequency transformer. Each FB p $(p = 1, 2, 3)$ is connected to a DC source p via a filter capacitor C_p. The total leakage inductance L_p ensures the power flow transfer between the ports. Using the Δ-type (Fig. 1-c) primary-

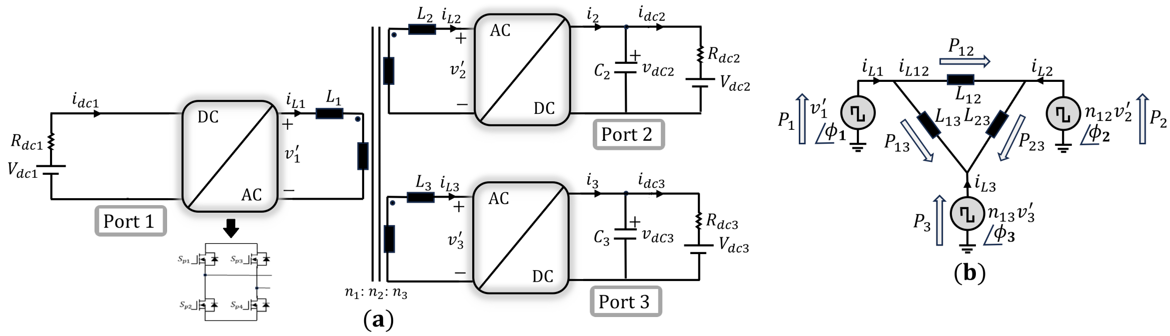

Fig. 1: (a) TAB DC-DC Converter, (b) Delta equivalent circuit.

referred equivalent circuit of the TAB converter and assuming that the losses are neglected, the power transfer between any two ports can be defined as follows:

$$P_{ij} = -P_{ji} = \frac{n_{ij} v_{dc_i} v_{dc_j}}{2\pi f_{sw} L_{ij}} \phi_{ij} \left(1 - \frac{|\phi_{ij}|}{\pi}\right) \tag{1}$$

where v_{dc_i} and v_{dc_j} are the voltages on the port i and port j respectively, $\phi_{ij} = \phi_j - \phi_i$ is the phase shift between port i and port j, $n_{ij} = \frac{n_j}{n_i}$ is the turn ratio of the j-th port with respect to the i-th port, L_{ij} the equivalent leakage inductance between port i and j defined by (2), and $L_i^{'} = \frac{L_i}{n_{ij}^2}$.

$$L_{ij} = L_i^{'} + L_j^{'} + \frac{L_i^{'} L_j^{'}}{L_k^{'}}, \quad k = 1,2,3 \quad \text{and} \quad k \neq i,j \tag{2}$$

As one can see from (1), the power flow transfer can be controlled by varying ϕ_{ij}. The power provided or received by each port is defined by (3). In order to guarantee energy conservation, the total power should be equal to zero (4).

$$P_i = \sum_{j=1}^{3} P_{ij} = \sum_{\substack{j=1\\ j\neq i}}^{3} \frac{n_{ij} v_{dc_i} v_{dc_j}}{\omega_{sw} L_{ij}} \phi_{ij} \left(1 - \frac{|\phi_{ij}|}{\pi}\right), \forall i \in \{1,2,3\} \tag{3}$$

$$\sum_{i=1}^{3} P_i = 0 \tag{4}$$

The current i_i (5) at port i is defined by dividing the power P_i (3) by the voltage v_{dc_i}.

$$i_i = \frac{P_i}{v_{dc_i}} = \sum_{\substack{j=1\\ j\neq i}}^{3} \frac{n_{ij} v_{dc_j}}{\omega_{sw} L_{ij}} \phi_{ij} \left(1 - \frac{|\phi_{ij}|}{\pi}\right), \qquad \forall i \in \{1,2,3\} \tag{5}$$

A. Reduced Order Model

In this subsection, a reduced order model (ROM) is developed for the TAB converter, neglecting the high-frequency dynamics of the transformer currents and simplifying its analysis by focusing on the dominant slow-frequency dynamics of the output filter capacitors . Applying Kirchhoff's laws to port i ($i = 2, 3$), the converter dynamics are described by:

$$\frac{dv_{dc_i}}{dt} = \frac{i_i}{C_i} - \frac{i_{dc_i}}{C_i}, \qquad \forall i \in \{2,3\} \tag{6}$$

$$v_{dc_i} = V_{dc_i} + R_{dc_i} i_{dc_i}, \qquad \forall i \in \{2,3\} \tag{7}$$

By deriving (7) and substituting (6) and (5) , the DC output current dynamics at each port is given by the following first and ROM:

$$\dot{i}_{dc_i} = \sum_{\substack{j=1\\ j\neq i}}^{3} \frac{n_{ij} v_{dc_j}}{\omega_{sw} L_{ij} C_i R_{dc_i}} \phi_{ij} \left(1 - \frac{|\phi_{ij}|}{\pi}\right) - \frac{i_{dc_i}}{C_i R_{dc_i}} \tag{8}$$

III. Proposed Control Design

Due to the non-linear and variable structure nature of power converters, linear control strategies are unable to provide satisfactory performance under large disturbances and parametric uncertainties. Sliding mode control (SMC) is particularly well-suited for these converters due to its inherent robustness, fast dynamic response, and design simplicity [15]. In this section, the SMC law is first designed to establish a baseline sliding manifold and ensure nominal stability and convergence. Then, as a second step, a RBFNN is integrated to adaptively approximate disturbances such as cross-coupling effects and unknown system dynamics and compensate for them in real time. This two-steps approach preserves the robust features of conventional SMC while improving transient recovery, enhancing stability, and reducing dependence on accurate system parameters [16]–[18].

A. Sliding mode control

Before proceeding to the SMC law design for each TAB converter's port, the dynamic model of the TAB converter is reformulated into a more convenient form. First, an auxiliary control variable u_i is introduced, which relates to the phase shift ϕ_{1i} through the following nonlinear transformation:

$$u_i = \phi_{1i} \left(1 - \frac{|\phi_{1i}|}{\pi}\right), \quad \forall i \in \{2,3\} \tag{9}$$

Conversely, ϕ_{1i} can be obtained from u_i via the inverse mapping:

$$\phi_{1i} = \begin{cases} \frac{\pi}{2}\left(1 - \sqrt{1 - \frac{4u_i}{\pi}}\right), & 0 \leq u_i < \frac{\pi}{4} \\ -\frac{\pi}{2}\left(1 - \sqrt{1 + \frac{4u_i}{\pi}}\right), & -\frac{\pi}{4} \leq u_i < 0 \end{cases} \tag{10}$$

Using this transformation, the TAB ROM (8) can be written in the following form:

$$\dot{y}_i = b_{0,i}u_i + f_i \tag{11}$$

where u_i is the control input defined by (9), $y = i_{dc_i}$ is the output current at port i to be controlled, $b_{0,i}$ (12) is a known control gain, and f_i (13) represents the lumped total disturbance, including cross-coupling effects, internal dynamics, and parametric uncertainties.

$$b_{0,i} = -\frac{n_{1i}v_{dc_1}}{\omega_{sw}L_{ij}C_iR_{dc_i}}, \quad \forall i \in \{2,3\} \tag{12}$$

$$f_i = \frac{n_{ij}v_{dc_j}\phi_{ij}(1-\frac{|\phi_{ij}|}{\pi})}{\omega_{sw}L_{ij}C_iR_{dc_i}} - \frac{i_{dc_i}}{C_iR_{dc_i}}, \forall i,j \in \{2,3\} \wedge i \neq j. \tag{13}$$

The controller design follows a two-stage procedure. First, a sliding surface σ_i, defined by (14), is selected to guarantee zero steady-state tracking error. Second, a control law is designed to drive the system's trajectories toward and maintain them on this surface, ensuring the desired asymptotic dynamics.

$$\sigma_i = e_i + \alpha_i \int e_i, \quad \forall i \in \{2,3\} \tag{14}$$

In (14), $e_i = y_{i,\text{ref}} - y_i$ is the tracking error, $y_{i,\text{ref}}$ is the reference output current, and $\alpha_i > 0$ is the integral sliding gain. To ensure stability on the sliding surface, the existence condition of the sliding mode given by (15) must be fulfilled.

$$\lim_{\sigma_i \to 0} \sigma_i \dot{\sigma}_i < 0 \tag{15}$$

To satisfy this condition, an exponential reaching law is adopted, defined as:

$$\dot{\sigma}_i = -\beta_i\sigma_i - \eta_i \text{sign}(\sigma_i) \tag{16}$$

where $\beta_i, \eta_i > 0$ are the gains controlling convergence, and $\text{sign}(\sigma_i)$ is the sign function.

Differentiating (14) and setting it equal to (16) yields the control law given by

$$u_i = \frac{1}{b_{0,i}}(-f_i + \alpha_i e_i + \beta_i\sigma_i + \eta_i \text{sign}(\sigma_i)) \tag{17}$$

After designing the control law, it is essential to analyze the stability of the closed-loop system by defining a quadratic $Lyapunov$ function candidate (18) for each port— the sum of which serves as the total $Lyapunov$ function for the entire system — as the basis for assessing the system's dynamic behavior.

$$V_i = \frac{1}{2}\sigma_i^2, \quad \forall i \in \{2,3\} \tag{18}$$

Taking the derivative of (18) with respect to time and substituting (17) results in $\dot{V}_i$ given by

$$\dot{V}_i = -\beta_i\sigma_i^2 - \eta_i|\sigma_i| \tag{19}$$

Since $\beta_i > 0$ and $\eta_i > 0$, it follows that $\dot{V}_i < 0$ for all $\sigma_i \neq 0$. This satisfies the *Lyapunov stability criterion*, ensuring asymptotic convergence to the sliding manifold $\sigma_i = 0$ and guaranteeing the asymptotic stability of the system.

B. RBF Neural Network Approximation

The effectiveness of the SMC law given in (17) relies critically on accurate estimation and cancellation of the lumped disturbance f_i (13). To address this requirement, an RBFNN is adopted to approximate f_i with high precision, thereby enabling effective mitigation of cross-coupling among the TAB converter ports. The RBFNN architecture, depicted in Fig. 2, consists of three layers: an input layer, a hidden layer with Gaussian activation functions, and a linear output layer. For each port of the TAB converter, the RBFNN is implemented online, employing the following network algorithm:

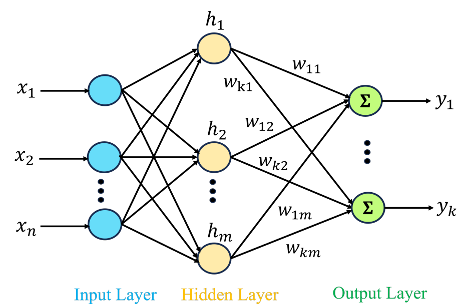

Fig. 2: RBF neural network architecture.

$$\begin{cases} h_j(x_i) = \exp\left(-\frac{\|x_i - \mathbf{c}_j\|^2}{2b_j^2}\right) \\ f_i = W_i^{*T}h_i(x_i) + \varepsilon_i \end{cases} \tag{20}$$

where x_i is the input vector defined as the tracking error (21), m is the number of hidden layer nodes, $j = 1, 2, \ldots, m$ is the j^{th} neuron node in the hidden layer, $h_i(x_i) \in \mathbb{R}^m$ is the Gaussian basis function vector, $\mathbf{c}j$ is the center point vector, b_j is the width vector, W_i^* is the optimal weight vector, and ε_i is the bounded approximation error satisfying $|\varepsilon_i| \leq \varepsilon_{i,\text{max}}$.

$$x_i = e_i \qquad \forall i \in \{2,3\} \tag{21}$$

In this paper, a single-hidden-layer RBFNN architecture with $m = 10$ neurons is adopted to achieve favorable trade-off between control performance and computational efficiency.

The total disturbance is approximated by the RBF NN as

$$\hat{f}_i = \hat{W}_i^T h(x_i) \tag{22}$$

and the approximation error is:

$$\tilde{f}_i = f_i - \hat{f}_i = \tilde{W}_i^T h_i(x_i) + \varepsilon_i, \quad |\varepsilon_i| \leq \varepsilon_{i,max} \tag{23}$$

where $\varepsilon_{i,max} > 0$ and $\tilde{W}_i = W_i^* - \hat{W}_i$. Substituting (22) into (17), the control law is re-defined as:

$$u_i = \frac{1}{b_{0,i}}\left(-\hat{f}_i + \alpha_i e_i + \beta_i\sigma_i + \eta_i \,\text{sign}(\sigma_i)\right) \tag{24}$$

In order to reduce the chattering effect, the $\text{sign}(\sigma_i)$ function in the controller (24) is replaced by saturation function $\text{sat}(\frac{\sigma_i}{\Delta_i})$. Consequently, the new SMC law is defined as

$$u_i = \frac{1}{b_{0,i}}\left(-\hat{f}_i + \alpha_i e_i + \beta_i\sigma_i + \eta_i \,\text{sat}\left(\frac{\sigma_i}{\Delta_i}\right)\right) \tag{25}$$

where $\Delta_i > 0$ is the boundary layer thickness, and sat$(\cdot)$ is saturation function. Substituting (25) into the sliding mode dynamics and using (23) yields:

$$\dot{\sigma}_i = -\tilde{W}_i^T h_i(x_i) - \varepsilon_i - \beta_i \sigma_i - \eta_i \mathrm{sat}\left(\frac{\sigma_i}{\Delta_i}\right) \tag{26}$$

To prove the stability of the integrated system, we define a composite Lyapunov function that includes both the sliding surface and the weight estimation error:

$$V = \sum_{i=2}^{3} \left(\frac{1}{2}\sigma_i^2 + \frac{1}{2\gamma_i}\tilde{W}_i^T \tilde{W}_i\right), \qquad \gamma_i > 0 \tag{27}$$

Differentiating (27) with respect to time, substituting (26), and noting that $\dot{\tilde{W}}_i = -\dot{\hat{W}}_i$, we obtain:

$$\begin{aligned} \dot{V} = \sum_{i=2}^{3} \Bigg(& -\sigma_i \tilde{W}_i^T h_i(x_i) - \sigma_i \varepsilon_i - \beta_i \sigma_i^2 \\ & -\eta_i \sigma_i \mathrm{sat}\left(\frac{\sigma_i}{\Delta_i}\right) - \frac{1}{\gamma_i}\tilde{W}_i^T \dot{\hat{W}}_i \Bigg) \end{aligned} \tag{28}$$

The adaptation law is chosen to cancel the $\tilde{W}_i$ term:

$$\dot{\hat{W}}_i = -\gamma_i \sigma_i h_i(x_i) \tag{29}$$

Substituting (29) into (28) simplifies to:

$$\dot{V} = \sum_{i=2}^{3} \left(-\sigma_i \varepsilon_i - \beta_i \sigma_i^2 - \eta_i \sigma_i \mathrm{sat}\left(\frac{\sigma_i}{\Delta_i}\right)\right) \tag{30}$$

The stability analysis is carried out for distinct operational boundaries based on Δ_i:

a) Outside the Boundary Layer ($|\sigma_i| > \Delta_i$)*:* Here sat$\left(\frac{\sigma_i}{\Delta_i}\right) = \mathrm{sign}(\sigma_i)$, so $\sigma_i$sat$\left(\frac{\sigma_i}{\Delta_i}\right) = |\sigma_i|$. Hence

$$\begin{aligned} \dot{V} &= \sum_{i=2}^{3} \left(-\beta_i \sigma_i^2 - \eta_i |\sigma_i| - \sigma_i \varepsilon_i\right) \\ &\leq \sum_{i=2}^{3} \left(-\beta_i \sigma_i^2 - (\eta_i - \varepsilon_{i,\max})|\sigma_i|\right) \end{aligned} \tag{31}$$

Since $\beta_i > 0$, ensuring that the robust switching control gains are strictly designed such that $\eta_i > \varepsilon_{i,\max}$ guarantees that $\dot{V} < 0$ for all $|\sigma_i| > \Delta_i$. This forces the system states to reach the boundary layer in finite time.

b) Inside the Boundary Layer ($|\sigma_i| \leq \Delta_i$)*:* Here sat$(\frac{\sigma_i}{\Delta_i}) = \frac{\sigma_i}{\Delta_i}$, giving

$$\dot{V} = \sum_{i=2}^{3} \left[-\left(\beta_i + \frac{\eta_i}{\Delta_i}\right)\sigma_i^2 - \sigma_i \varepsilon_i\right] \tag{32}$$

Applying Young's Inequality to the bounded approximation error term yields $-\sigma_i \varepsilon_i \leq \frac{\kappa_i}{2}\sigma_i^2 + \frac{1}{2\kappa_i}\varepsilon_{i,\max}^2$, where $\kappa_i > 0$ is a positive design scalar. Substituting this back into (32)) isolates the boundary bounds:

$$\dot{V} \leq \sum_{i=2}^{3} \left[-\left(\beta_i + \frac{\eta_i}{\Delta_i} - \frac{\kappa_i}{2}\right)\sigma_i^2 + \frac{1}{2\kappa_i}\varepsilon_{i,\max}^2\right] \tag{33}$$

By selectively setting the parameter arrays to satisfy $\left(\beta_i + \frac{\eta_i}{\Delta_i}\right) > \frac{\kappa_i}{2}$, Equation (33) guarantees that $\dot{V} \leq 0$ whenever the sliding variable state leaves the compact residual boundary set defined by:

$$|\sigma_i| > \sqrt{\frac{\varepsilon_{i,\max}^2}{\kappa_i\left(2\beta_i + \frac{2\eta_i}{\Delta_i} - \kappa_i\right)}} \tag{34}$$

According to the extended Lyapunov theorem, this structurally proves that practical tracking stability is achieved inside the boundary envelope Δ_i, while the weights $\hat{W}_i$ are guaranteed to remain strictly bounded.

IV. Simulation Results and Discussion

Using MATLAB/Simulink, numerical simulations are conducted to evaluate the performance of the hybrid RBFNN–SMC controller (Fig. 3). The parameters of the overall system are listed in Table I. To assess the performance, four distinct operating modes are examined: 1) Port 1 supplies both ports 2 and 3; 2) Port 1 supplies port 2 with port 3 disconnected; 3) Port 3 supplies port 2 with port 1 disconnected; and 4) Ports 2 and 3 supply port 1. Throughout these operation modes (Fig. 4-a), the RBFNN-SMC successfully ensures accurate power sharing and highlights the bidirectional versatility of the TAB converter. Most importantly, the adaptive nature of the RBFNN effectively learns and mitigates the non-linear cross-coupling effects between the ports in real-time by predicting the lumped disturbance. Consequently, the control signal, illustrated in Fig. 4-b, remains smooth and free of chattering throughout the simulation. The benefits of this smooth control extend to the sliding dynamics (σ_i), as illustrated by the 3D phase-space trajectories of the sliding manifolds in Fig. 5. Upon a step change in the power reference, the state trajectories are quickly driven to the sliding planes ($\sigma_i = 0$) during the reaching phase, after which, they slide smoothly along the ideal tracking line toward the origin, demonstrating the excellent transient performance of the adaptive mechanism. To validate the effectiveness and robustness of the proposed hybrid RBFNN-SMC strategy, a comparative study was conducted with a conventional SMC and a linear

TABLE I: TAB Converter and controllers' parameters

Parameter	Value
Rated power: P_2, P_3	5, 5 kW
Port voltage: V_{dc1}, V_{dc2}, V_{dc3}	800, 400, 400 V
Internal resistance: R_{dc1}, R_{dc2}, R_{dc3}	0.25, 0.25, 0.25 Ω
Transformer turns ratio: n_1:n_2:n_3	1 : 0.5 : 0.5
Port inductance: L_1, L_2, L_3	80, 80, 80 µH
Port capacitance: C_2, C_3	2500, 2500 µF
Switching frequency: f_{sw}	10 kHz
RBFNN-SMC for port i:	
α_i, β_i, η_i, Δ_i	260, 8000, 300, 0.1
Nº of neurons in the input layer	1
Nº of neurons in the hidden layer	10
Nº of neurons in the output layer	1
PI-based IDM	k_{pi}, k_{ii}, 10^{-4}, 50

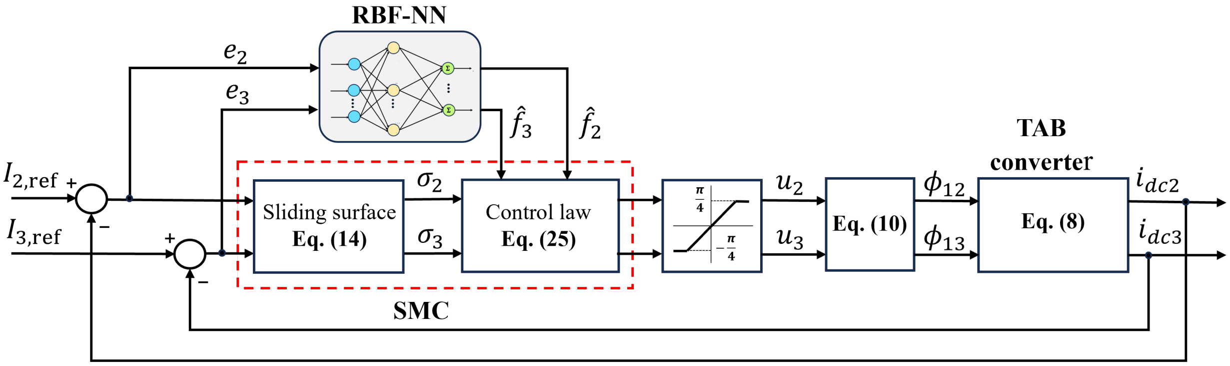

Fig. 3: Block diagram of the TAB converter RBFNN-SMC system.

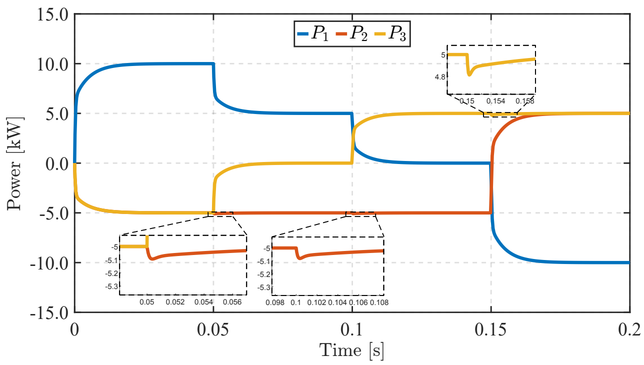

(a) Power sharing among the three ports

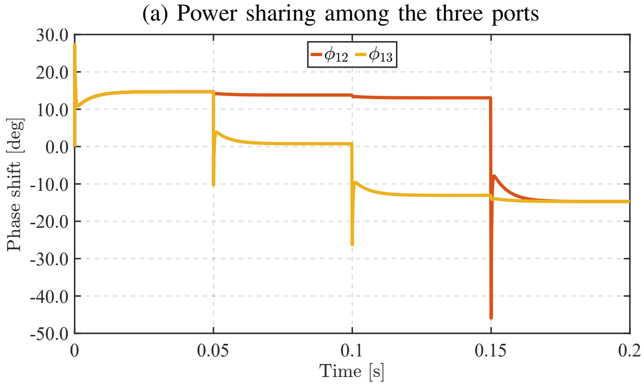

(b) Control signal

Fig. 4: Dynamic response of the TAB converter across four consecutive operation modes.

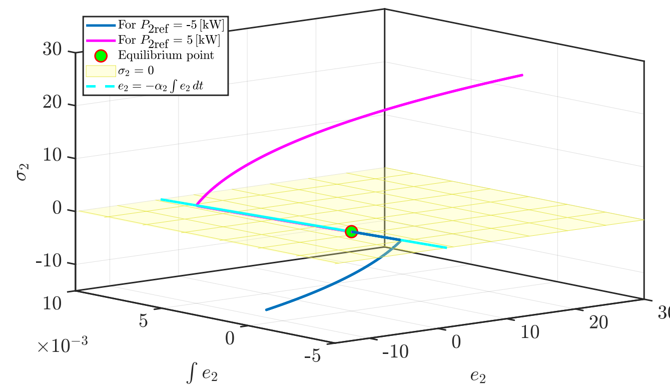

(a) Port 2 sliding manifold σ_2

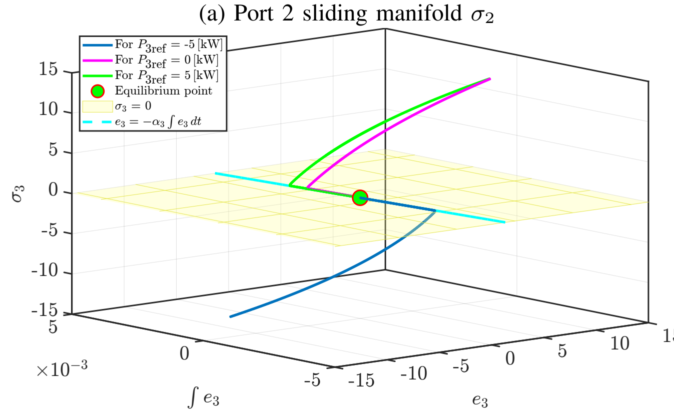

(b) Port 3 sliding manifold σ_3

Fig. 5: 3D phase-space trajectories of the sliding manifolds under power step changes.

PI-based controller employing an inverted decoupling matrix (IDM). While the PI-IDM approach is widely used for its simplicity, its theoretical details—such as small-signal modeling and decoupling matrix synthesis—are not elaborated here; the reader is encouraged to refer to references [5]- [8] for an in-depth discussion. The control strategies are evaluated under three consecutive nominal disturbances: 1) 50% load decrease at port 3 ($t = 0.15\,$s), 2) 20% input voltage drop ($t = 0.3\,$s), and 3) 100% leakage inductance deviation at port 2 ($t = 0.45\,$s). As shown in Fig. 6b, the proposed RBFNN-SMC significantly outperforms both benchmark controllers, achieving the fastest convergence and the most robust disturbances rejection. Conventional SMC provides stable but slower convergence than the RBFNN-SMC, while the PI-based IDM shows the largest overshoot and longest settling time, especially under inductance deviation. By approximating the coupling terms dynamically, it maintains the highest precision even during the most severe mode transitions. These findings confirm that the adaptive learning capability of the RBF neural network enhances the robustness of the sliding mode controller against parametric uncertainties and external disturbances.

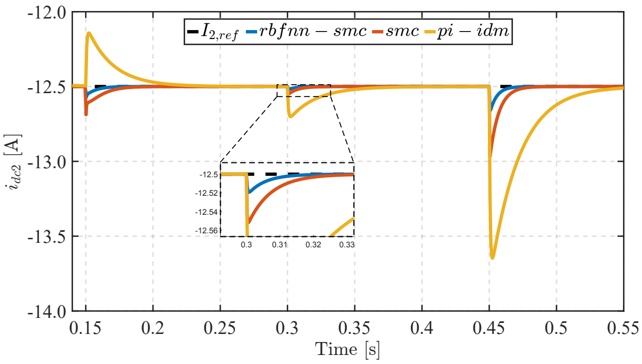

(a) Port 2

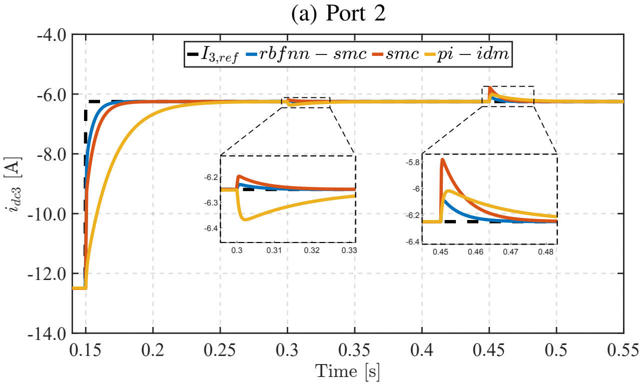

(b) Port 3

Fig. 6: Output current response subject to three disturbances: load variation P_2 at port 2, input voltage V_{dc1} drop at port 1, and leakage inductance L_2 deviation at port 2.

V. Conclusion

This paper investigates a robust hybrid RBFNN-SMC strategy for cross-coupling mitigation in a TAB converter. The design process began with a conventional SMC based on a reduced-order model; then, an RBFNN was used online to adaptively estimate and cancel the lumped disturbance term representing cross-coupling effects and system uncertainties. Using a quadratic total Lyapunov function, the stability of the closed-loop system has been proven. Simulation results obtained under four operating mode scenarios validate the controller's effectiveness in achieving precise power sharing and decoupled power flow. A comparative evaluation with conventional SMC and PI-based IDM controllers under parametric uncertainties and external disturbances demonstrates that the proposed RBFNN-SMC outperforms both benchmarks, exhibiting faster convergence and superior robustness.

Acknowledgment

The work was partially funded by the European Union's Horizon Europe Research and Innovation Program for i-PLUG project with grant agreement nº101069770 and from the Universities Department of Catalonia Government under FI2024 program with grant agreement 2024-FIB-00930.

References

[1] J. L. Duarte, and M. Hendrix, and M. G. Simões, "Familly of multiport bidirectional DC-DC converters," IEE Proce. - Elec. Power App., vol.15, pp.451–487, 2006.

[2] T. Pereira, and F. Hoffmann, and R. Zhu,and M. Liserre, "A comprehensive assessment of multiwinding transformer-based DC–DC converters," IEEE Trans. Power Elec., vol. 36, pp. 10020–10036, 2021.

[3] J. L. Duarte, and M. Hendrix, and M. G. Simões, "Three-port bidirectional converter for hybrid fuel cell systems," IEEE Trans. Power Elec., vol. 22, pp. 480–487, 2007.

[4] R. W. De Doncker, and D. M. Divan, and M. H. Kheraluwala, "A three-phase soft-switched high-power-density DC/DC converter for high-power applications," IEEE Trans. Ind. Appl., vol. 27, no. 1, pp. 63-73, Jan. 1991.

[5] P. Koohi, and A. J. Watson, and J. C. Clarea, nd T. B. Soeiro, and P. W. Wheeler, "A Survey on Multi-Active Bridge DC-DC Converters: Power Flow Decoupling Techniques, Applications, and Challenges," Energies, vol. 16, pp. 5927–5974, 2023.

[6] A. C. Henao-Mu$\bar{n}$oz, and M. B. Debbat, and A. Pepiciello, and J. L. Dom$\acute{i}$nguez- Garc$\acute{i}$a, "Triple Active Bridge Modeling and Decoupling Control," Electronics, vol. 14, no. 2, pp.4224–, 2025.

[7] R. Tarraf, and D. Frey, S. Leirens, and S. Carcouet,X. Maynard, and Y. Lembeye, "Modeling and Control of a Hybrid-Fed Triple-Active Bridge Converter," Energies, vol. 16, no. 16, 2023.

[8] C. Zhao, and S. D. Round, and J. W. Kolar, "An Isolated Three-Port Bidirectional DC-DC Converter With Decoupled Power Flow Management," IEEE Trans. Power Elect., vol. 23, pp.2443–2453, 2008.

[9] N. Koya, and K. Yuichi, and w. Keiji, "Implementation of Decoupling Power Flow Control System in Triple Active Bridge Converter Rated at 400V, 10kW, and 20kHz," IEEJ Jour. Indus. Appl., vol. 7, pp. 410–415, 2018.

[10] M. B. Debbat, A. C. Henao-Mu$\bar{n}$oz, and A. Pepiciello, and J. L. Dom$\acute{i}$nguez- Garc$\acute{i}$a, "Sliding-Mode Based Control Technique for Triple Active Bridge DC-DC Converter," IEEE XV Inter. Symp. Indus. Elect. Appl. (INDEL), pp. 1–6, Banja Luka, Bosnia and Herzegovina, 2024.

[11] S. Bandyopadhyay, and Z. Qin, and P. Bauer, "Decoupling Control of Multiactive Bridge Converters Using Linear Active Disturbance Rejection," IEEE Trans. Indus. Elect., vol. 68, no. 11, pp. 10688–10698, 2021.

[12] A. H. A. Adam, and J. Chen, and S. Kamel, and E. M. Ahmed, Z. A. Zaki, "Improved dynamic performance of triple active bridge DC-DC converter using differential flatness control for more electric aircraft applications," Results in Engineering, vol. 23, pp.102811–102832 2024.

[13] G. Buticchi, and A. Farjudian, and J. Oh, and L. Tarisciotti, "An ANN-Assisted Control for the Power Decoupling of a Multiple Active Bridge DC-DC Converter," IEEE 48^{th} Ann. Conf. Indus. Elect. Soc. (IECON), Brussels, Belgium; 2022.

[14] Q. Rongxin, and G. Chunyang, and L. Jing, and Y. Jiajun, "A Simplified ANN Based Power Decoupling Method of MAB Converters," IEEE 8^{th} Inter. Elect. Ener. Conf. (CIEEC). Changsha, China, 2025.

[15] V. I. Utkin, "Sliding mode control design principles and applications to electric drives," IEEE Trans. Ind. Elect., vol. 40, no. 1, pp.6783–6800, 1993.

[16] J. Sun, C. Chen and H. Wei, "RBF Neural Network-Enhanced Adaptive Sliding Mode Control for VSG Systems with Multi-Parameter Optimization," Electronics, 2025, vol. 14, no. 21, pp. 4309.

[17] S. Lian, Y. Sun, and W. Zhang, "A sliding mode control strategy based on RBF neural network for grid-connected inverter," in IEEE 7^{th} Inter. Conf. Energy Syst. and Elec. Power (ICESEP), Wuhan, China, 2025.

[18] X. Xiao, J. Lv, Y. Chang, J. Chen and H. He *et al.*, "Adaptive sliding mode control integrating with RBFNN for proton exchange membrane fuel cell power conditioning," Appl. Sci., 2022, vol. 12, no. 6, pp. 3132.